Particles II

Access the latest eBook →

11 Advanced Optical Metrology

Particles II

EVIDENT OLYMPUS

WILEY

Impact on Biological Systems and the Environment

This eBook is dedicated to the research of Professor David Wertheim.
In collaboration with various groups, Professor Wertheim uses confocal microscopy to analyse the impact of different types of particles on human health and the environment, with a focus on human health-hazardous particles detected with solid-state nuclear track detectors (SSNTD). Download for free, today.

EVIDENT OLYMPUS

WILEY

Sulfur Treatment Passivates Bulk Defects in Sb$_2$Se$_3$ Photocathodes for Water Splitting

Rajiv Ramanujam Prabhakar, Thomas Moehl, Dennis Friedrich, Marinus Kunst, Sudhanshu Shukla, Damilola Adeleye, Vinayaka H. Damle, Sebastian Siol, Wei Cui, Laxman Gouda, Jihye Suh, Yaakov R. Tischler, Roel van de Krol, and S. David Tilley*

Sb$_2$Se$_3$ has emerged as an important photoelectrochemical (PEC) and photovoltaic (PV) material due to its rapid rise in photoconversion efficiencies. However, Sb$_2$Se$_3$ has a complex defect chemistry, which reduces the maximum photovoltage. Thus, it is important to understand these defects and develop defect passivation strategies in Sb$_2$Se$_3$. A comprehensive investigation of the charge carrier dynamics of Sb$_2$Se$_3$ and the influence of sulfur treatment on its optoelectronic properties is performed using time-resolved microwave conductivity (TRMC), photoluminescence (PL) spectroscopy, and low-frequency Raman spectroscopy (LFR). The key finding in this work is that upon sulfur treatment of Sb$_2$Se$_3$, the carrier lifetime is increased by the passivation of deep defects in Sb$_2$Se$_3$ in both the surface region and the bulk, which is evidenced by increased charge carrier lifetime of TRMC decay dynamics, increased radiative recombination efficiency, decreased deep defect level emission (PL), and the emergence of new vibration modes by LFR.

R. R. Prabhakar, T. Moehl, M. Kunst, W. Cui, L. Gouda, J. Suh, S. D. Tilley
Department of Chemistry
University of Zurich
Winterthurerstrasse 190, Zurich CH-8057, Switzerland
E-mail: david.tilley@chem.uzh.ch

D. Friedrich, R. van de Krol
Institute for Solar Fuels
Helmholtz-Zentrum Berlin für Materialien und Energie GmbH
Hahn-Meitner-Platz 1, 14109 Berlin, Germany

S. Shukla, D. Adeleye
Laboratory for Photovoltaics
Department of Physics and Materials Science
University of Luxembourg
Belvaux L-4422, Luxembourg

V. H. Damle, Y. R. Tischler
Device Spectroscopy Laboratory
Department of Chemistry
Institute for Nanotechnology & Advanced Materials
Bar-Ilan University
Ramat Gan 5290000, Israel

S. Siol
Empa Swiss Federal Laboratories for Materials Science and Technology
Überlandstrasse 129, Dübendorf CH-8600, Switzerland

1. Introduction

Photovoltaic (PV) and photoelectrochemical (PEC) cells based on Sb$_2$Se$_3$ have seen a rapid rise in interest in recent years and significant progress has been made in their power conversion efficiencies,[1,2] which is primarily due to its high absorption coefficient and excellent optoelectronic properties. However, a major challenge for Sb$_2$Se$_3$ is the low photovoltage obtained from such devices. Originally it was thought that Sb$_2$Se$_3$ would exhibit low defect concentration as it is a binary compound (better stoichiometric control) with benign grain boundaries.[3] However, recent computational studies have shown the complex defect chemistry of Sb$_2$Se$_3$ and the formation of deep defect states that are detrimental to PV/PEC performance.[4] Cation–anion anti-site defects have been shown to have a low formation energy and are energetically positioned close to the mid gap, serving as deep recombination centers. Therefore, the understanding and the suppression/passivation of such deep defects is crucial for the further development of Sb$_2$Se$_3$ as a PV/PEC material. Several strategies have been presented in the literature such as Te incorporation for defect passivation,[5] sulfurization treatment for improved photovoltage,[6] and gradient sulfur doping in Sb$_2$Se$_3$.[7] More fundamental insights into the basic optoelectronic properties for defect passivation/suppression for Sb$_2$Se$_3$, however, have not yet been reported.

In this work, we employed time-resolved microwave conductivity (TRMC) and photoluminescence (PL) spectroscopy to gain understanding of the passivation of defects in Sb$_2$Se$_3$ by sulfur treatment. We investigated the charge carrier dynamics of Sb$_2$Se$_3$ before and after sulfur treatment using TRMC and observed the passivation of defects in Sb$_2$Se$_3$ as evidenced by longer carrier lifetimes of the initial photoconductance decay. The wavelength-dependent TRMC study also shows that the passivation of defects by the sulfur treatment reduces not only the surface recombination rate, but also the bulk recombination rate. Furthermore, we demonstrate increased radiative recombination efficiency by suppression of nonradiative recombination pathways in sulfur-treated Sb$_2$Se$_3$ using PL spectroscopy. In addition to this, low-frequency Raman spectroscopy (LFR) showed the emergence of new vibration modes, which indicate increased long-range order in

the Sb₂Se₃ semiconductor thin films upon sulfur treatment. These results explain the improved photovoltage of Sb₂Se₃ upon sulfur treatment, which presents a simple and efficient defect passivation strategy.

2. Results and Discussion

Sb₂Se₃ thin films were synthesized on quartz substrates by selenization of Sb metal. The sulfurization of these films was carried out in a sulfur atmosphere (see Experimental Section in Supporting Information for details). No significant surface morphological changes of Sb₂Se₃ thin films were observed upon sulfur treatment and incorporation of sulfur into the films was confirmed by EDX (Figure S1, Supporting Information). The XRD pattern of Sb₂Se₃ was indexed to the orthorhombic phase of Sb₂Se₃ (JCPDS 01-089-0821), and that of the sulfur-treated film was identical to the Sb₂Se₃ (Figure S2, Supporting Information), indicating that the Sb₂Se₃ crystal structure was not affected by the sulfurization treatment. The crystallite size as obtained from

the Scherrer equation was found to be 33.08 nm for the as-prepared Sb₂Se₃ film and 34.34 nm for the sulfur-treated sample, and the morphological differences between the two samples are minor. The onset of absorption does not change significantly with sulfur treatment indicating that the incorporation of sulfur does not change the optical bandgap (Figure S3, Supporting Information). For these reasons, and because we also do not observe Raman peaks for Sb₂S₃ (vide infra), the sulfur may be present between the Sb₂Se₃ ribbons in the interstitial space.

We investigated the charge carrier dynamics in Sb₂Se₃, and how sulfur treatment of Sb₂Se₃ affects the underlying carrier recombination processes using TRMC. In TRMC, photoexcited charge carriers are generated in a semiconductor by a short laser pulse, giving rise to a light-induced change in the conductance of the sample (ΔG, **Figure 1**a) as compared with the dark conductance. The microwave radiation is absorbed by free mobile charge carriers and the change of reflected microwave power, ΔP, after the laser pulse is proportional to the amount of light-induced mobile charge carriers and therefore the photoconductance:
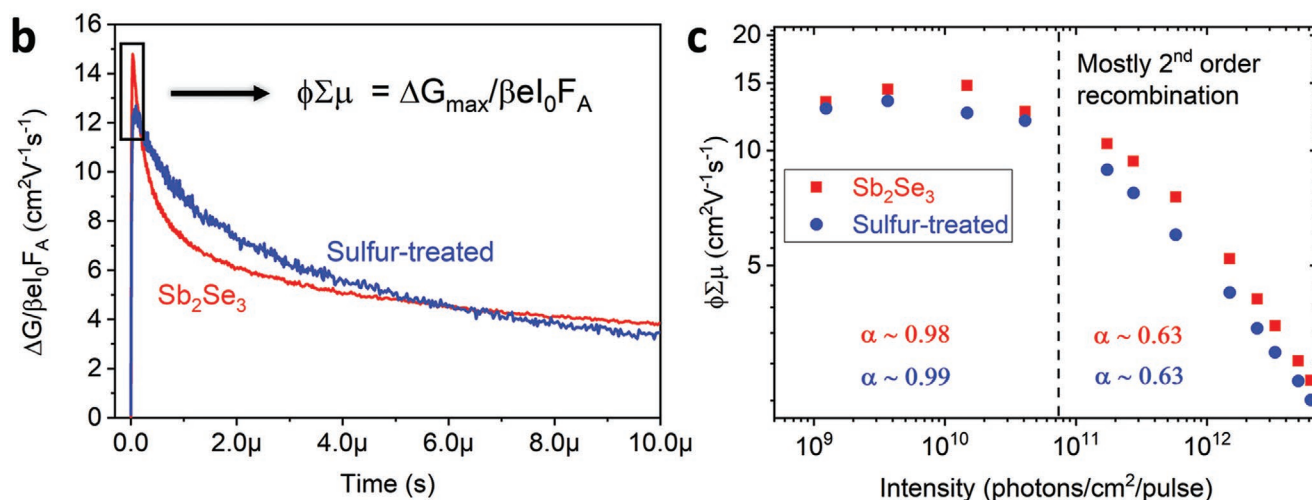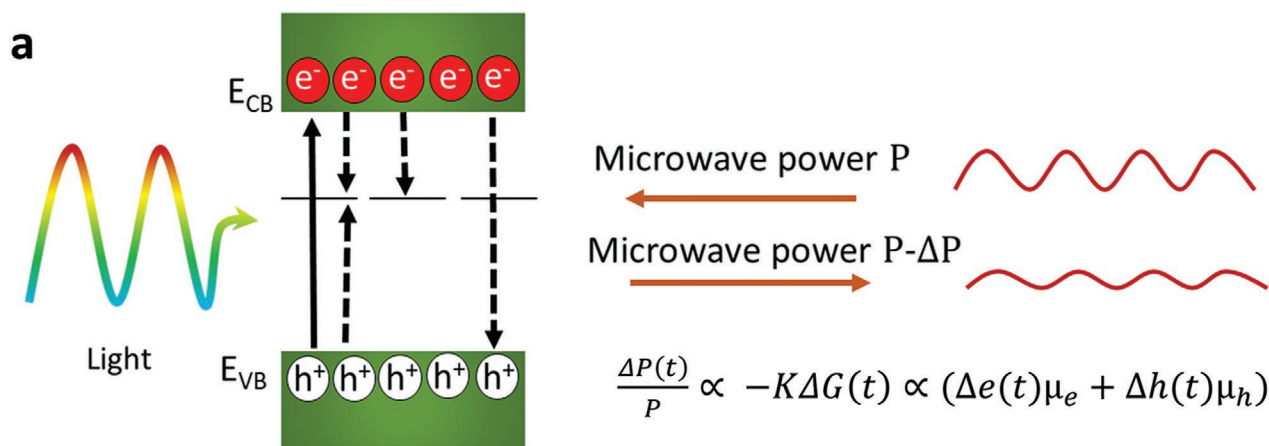

Figure 1. Photoconductance and recombination kinetics of Sb₂Se₃ and sulfur-treated films. a) Schematic illustrating the principle of TRMC. b) Transient photoconductance as a function of time induced by 500 nm laser light for 1.48×10^{10} photons cm⁻² pulse⁻¹ for Sb₂Se₃ and sulfur-treated films. c) $\phi\Sigma\mu$ as a function of the excitation density for Sb₂Se₃ and sulfur-treated films.

$$\frac{\Delta P(t)}{P} \propto -K\Delta G(t) \propto (\Delta e(t)\mu_e + \Delta h(t)\mu_h)$$

$$\phi\Sigma\mu = \Delta G_{max}/\beta e I_0 F_A$$

$$\frac{\Delta P(t)}{P} \propto -K \Delta G(t) \propto \left(\Delta e(t) \mu_e + \Delta h(t) \mu_h \right) \qquad (1)$$

with K being the sensitivity factor of the measurement setup, Δe and Δh the photoinduced change in free mobile charge carriers and their associated mobility μ_e and μ_h, respectively.[8,9] The microwave reflection and therefore also the photoconductance changes over time due to both radiative and nonradiative losses of free mobile charge carriers in the semiconductor and hence valuable information with regards to the loss mechanism of photogenerated charge carriers in the semiconductor can be obtained.

The bare Sb_2Se_3 and sulfur-treated films were excited with 3 ns pulses, with excitation wavelengths between 350 and 1100 nm at different intensities (10^9–10^{13} photons pulse^{-1} cm^{-2}) and a characteristic response time constant of the cavity of 20 ns. The change in photoconductance was monitored over time (ns to ≈80 µs). As there are no charge selective contacts to separate the charge carriers, and assuming that the carrier mobility does not change during the time window of our measurement, the decrease in the photoconductance with time is purely due to the decrease in the concentration of mobile carriers in the bands by trapping or annihilation by recombination.

It is convenient to analyze the TRMC data by distinguishing between the maximum photoconductance, ΔG_{max}, and the decay of the photoconductance, ΔG. ΔG_{max} reflects the mobilities of the charge carriers and the convolution of kinetic processes during the light excitation and the reaction time of the cavity. The decay of the photoconductance in contrast reflects the kinetic processes of free electron–hole pairs in the semiconductor, which undergo recombination or trapping.

Figure S4 (Supporting Information) shows the photoconductance normalized to the amount of photogenerated charge carriers ($\Delta G/\beta e I_0 F_A$) as a function of time under 500 nm (2.48 eV) pulsed illumination with a light intensity of 3.69×10^9 photons cm^{-2} per pulse (light intensity corresponding to ≈1 sun illumination) for Sb_2Se_3 and sulfur-treated films. From the peak of the TRMC signal (ΔG_{max}), we can estimate the sum of the mobilities of the individual carriers using the equation given below.[10]

$$\phi \sum \mu = \frac{\Delta G_{max}}{I_0 \beta e F_A} \qquad (2)$$

where I_0 is the incident intensity per pulse, e is the elementary charge, β is the ratio between the inner broad and narrow dimensions of the waveguide, F_A is the fraction of incident photons absorbed within the sample, ϕ is the charge carrier generation yield, and $\Sigma \mu$ is the sum of electron and hole mobilities (Figure 1b, see also the Supporting Information for a more detailed explanation of $\phi \Sigma \mu$ and ΔG).

The effective mobility for both Sb_2Se_3 and sulfur-treated films was greater than 10 cm^2 V^{-1} s^{-1}, which is considerably higher than other materials used in water splitting such as Fe_2O_3 (0.005 cm^2 V^{-1} s^{-1}),[11] $CuFeO_2$ (0.2 cm^2 V^{-1} s^{-1}),[12] and $BiVO_4$ (0.04 cm^2 V^{-1} s^{-1}).[13] Interesting to note is the fact that at a relatively low intensity of photons from the laser (≈10^9 photons cm^{-2} per pulse) clear TRMC signals could be detected

in contrast to the light intensities of >10^{13} photons cm^{-2} pulse^{-1} needed to detect signals from Fe_2O_3, $BiVO_4$, or $CuFeO_2$.[11–13] This observation already reveals the excellent optoelectronic properties and relatively low trap/defect density of Sb_2Se_3 as compared with other emerging light absorbers for PV or PEC applications.[14]

The maximum of the peak height of the photoconductance is very similar for the two different sample types (5–10% higher for the untreated sample). With the observation that the microwave reflection in the dark remained the same (i.e., the sulfur treatment does not dope the sample), we can conclude that the sulfur treatment did not substantially change the effective mobility values of the charge carriers.

When comparing the light intensity dependence of the maximum of the photoconductance signal normalized to the number of photons absorbed ($\phi \Sigma \mu$), it is observed that the TRMC signal is relatively constant at lower light intensities and then decreases with increasing light intensity >10^{11} photons cm^{-2} pulse^{-1} (Figure 1c). Based on the slope of the log plot $\phi \Sigma \mu$ versus $I_0^{\alpha-1}$, the order of the mobile charge carrier loss process could be deduced (where α is the reciprocal of the order of the recombination process).[13] At lower light intensities, the concentration of photogenerated electrons and holes is low, and the photoconductance signal is directly proportional to the amount of photons and therefore the generated electron–hole pairs. At light intensities above 10^{11} photons cm^{-2} pulse^{-1} α was ≈0.63, showing that second-order recombination plays a major role in the reduction of the maximum photoconductance signal. At these increased light intensities, the semiconductor bands are populated by a high density of photogenerated charge carriers leading to increased second-order recombination due to direct electron and hole recombination already during the laser pulse and the response time of the cavity, reducing ΔG_{max} (Figure 1c) significantly.

The decay of the photoconductance in our samples can be analyzed in two main time ranges (**Figure 2**a,b). The first range represents the period up to 70–100 ns after ΔG_{max} showing a fast initial decay (fast process) of the photogenerated charge carriers. This initial fast decay of the photoconductance gives way to an extended decay, which can be observed (with a similar slope for both sample types) in the linear part of the log-log plot in Figure 2b. An extended decay can be due to the different processes; but in non-crystalline or multi-crystalline semiconductors, it is mainly due to the interaction of mobile charge carriers with a wide distribution of states in the band tail.[15–17] Ultimately, the extended decay crosses over into an exponential type decay (>1 µs, labeled slow process decay in Figure 2b).

Comparing the fast decay process (up to ≈70–100 ns) for the two sample types, it is evident that the recombination rate is reduced in the sulfur-treated films (Figure 2a). As the decay could not be fitted with a double exponential over the whole time range (Figure S5, Supporting Information), we have separated the fitting of the decays into a fast and a slow component, each fitted with a single exponential (Figure 2c). The time constants of the fast processes could only be extracted for the higher light intensities (>10^{11} photons cm^{-2} pulse^{-1}; Figure S6, Supporting Information). At low light intensities (<10^{11} photons cm^{-2} pulse^{-1}), there was practically no change in the TRMC signal in the time range up to 70 ns (even up to 200 ns,
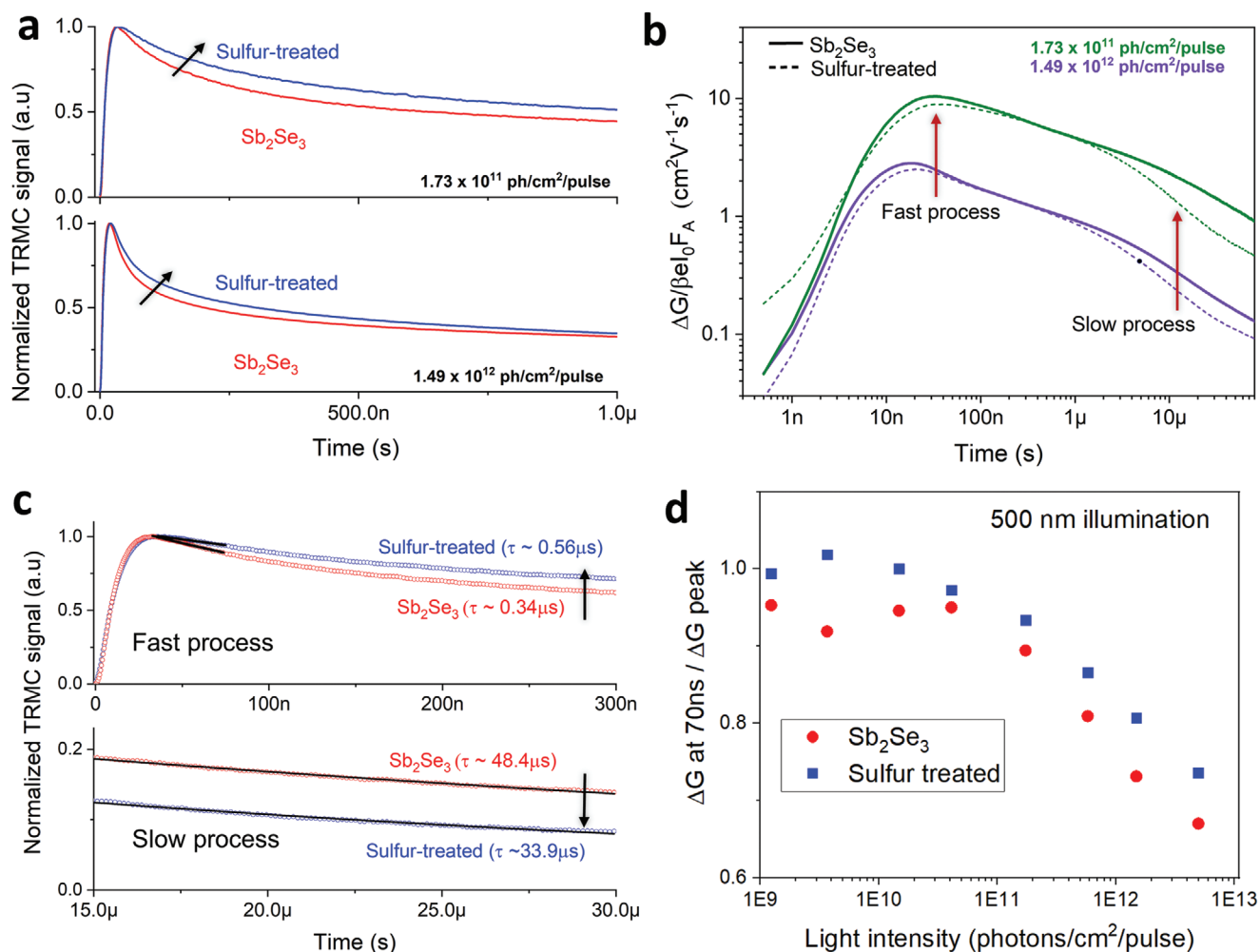
Figure 2. Lifetime of photoconductance decay processes in Sb_2Se_3 and sulfur-treated films. a) Normalized TRMC signal showing the longer lifetime of sulfur-treated films under 500 nm illumination. b) Double log plot for Sb_2Se_3 and sulfur-treated films showing the different decay processes taking place under 500 nm illumination. c) Exponential fitting to estimate the lifetime of the fast and slow processes under 500 nm illumination (1.73×10^{11} photons cm^{-2} $pulse^{-1}$). d) Ratio of the photoconductance signal ΔG at 70 ns and the ΔG peak as a function of light intensity.

see Figure S7, Supporting Information) and no exponential fit of the data could be performed. An alternative approach for a comparison of the fast decay under such conditions is to compare the signal height at 10 ns with the signal height at 70 ns. The quotient of the ΔG at 70 ns/ΔG peak qualitatively describes the decay properties/times sufficiently for the following discussion and interpretation (Figure 2d).[18,19] Clearly, the sulfur-treated sample shows a slower decay of photoconductance quotient, which is equivalent to a longer lifetime of the photogenerated charge carriers for the fast process (a similar result has been obtained by the exponential fitting procedure for the fast decay at higher light intensities, Figure S6, Supporting Information). The difference in the fast decay (time) between the Sb_2Se_3 and the sulfur-treated Sb_2Se_3 was observed over a range of light intensities and was independent of the excitation wavelength (Table S1, Supporting Information). The fact that the lifetime determined is in the same order of magnitude for both types of samples implies that they represent the same loss or recombination event of the free mobile charge carriers. A recombination process mediated by defects is the

most plausible explanation for the fast decay between 10 and 70 ns,[15,17] which is also the decay process normally assumed to be active under moderate stationary illumination conditions, i.e., in PV and PEC devices under "1 sun."

The slow decay in contrast is clearly faster for the sulfur-treated samples (Figure 2c; Table S2, Supporting Information), which on first sight appears to be a contradiction when compared to the initial fast decay. Normally such a slow decay can be explained either by i) a reduction of shallow traps or a narrower bandtail by the sulfur treatment, which in turn leads to a faster re-emission of trapped charge carriers (by thermalization) back into the bands followed by recombination, or ii) the formation of a trap with higher cross-section for recombination after sulfur treatment. TRMC cannot clearly differentiate between these two possibilities though the latter one is improbable since it would also appear in the fast decay process.

In **Figure 3**a,b, the maximum TRMC signal is compared for the different excitation wavelengths using front versus backside illumination. The shorter wavelengths exhibited significantly lower peak $\phi\Sigma\mu$ signal when illuminated from the back,
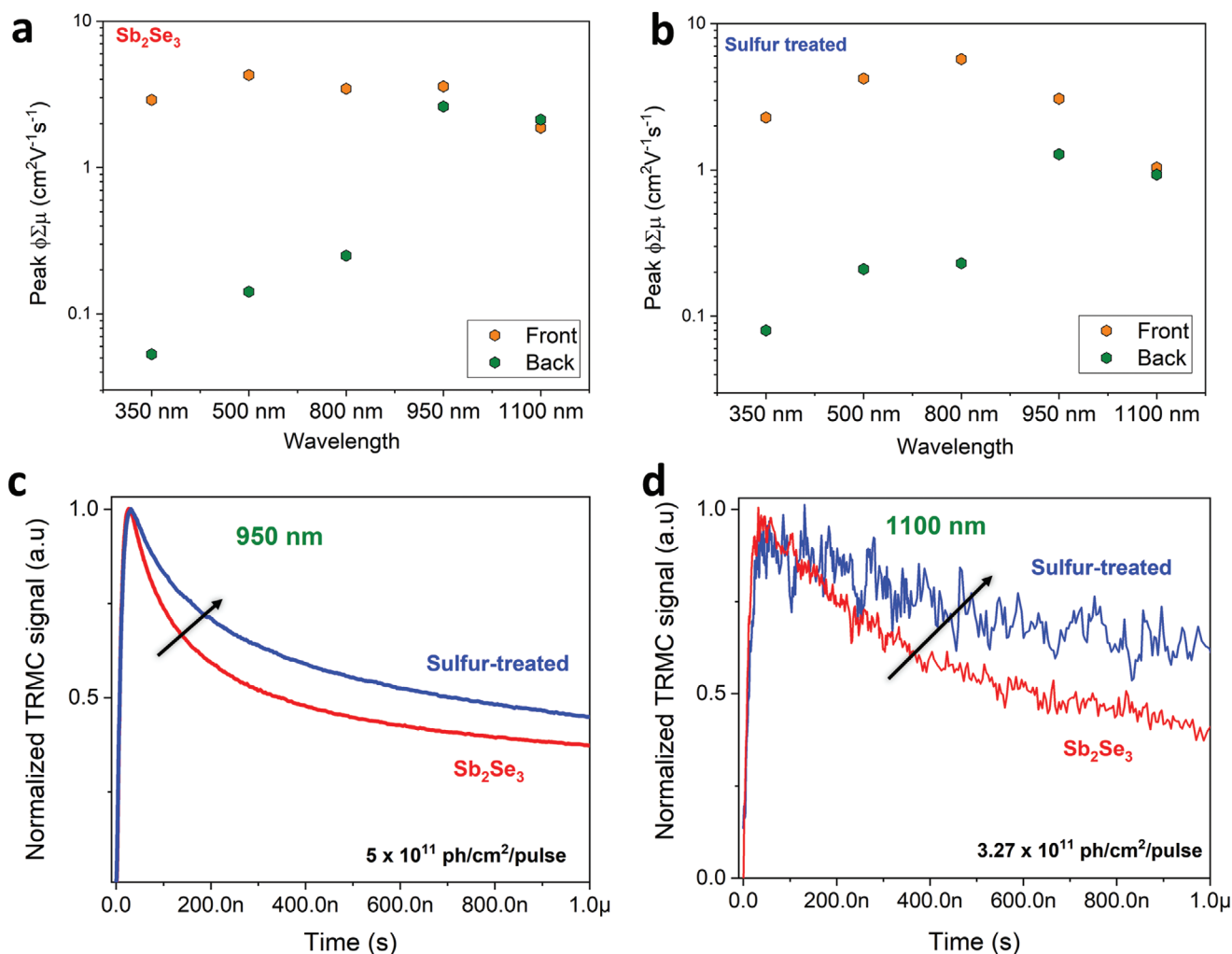
**ADVANCED
SCIENCE NEWS**

www.advancedsciencenews.com

**ADVANCED
FUNCTIONAL
MATERIALS**

www.afm-journal.de

Figure 3. Wavelength dependent TRMC decay dynamics Peak $\phi\Sigma\mu$ value versus wavelength plots for a) Sb_2Se_3 and b) sulfur-treated films for front versus back illumination (light intensity $\approx 2 \times 10^{12}$ photons cm^{-2} $pulse^{-1}$). Normalized TRMC signal plots for c) 950 nm and d) 1100 nm illumination of Sb_2Se_3 and sulfur-treated films.

which we attribute to a high recombination velocity at the back interface (quartz/Sb_2Se_3) due to a high defect density. With decreasing energy of the excitation wavelength, the penetration depth increases and the photogenerated charge carriers start to achieve an even distribution for both front and back illumination (Figure 3a,b). This observation implies that especially at 1100 nm the photoconductance signal originates mainly from the bulk of the semiconductor. Upon comparison of the TRMC decay of Sb_2Se_3 and sulfur-treated films for 1100 nm illumination, the sulfur-treated sample still exhibited a slower decay rate of the fast process than the Sb_2Se_3 sample (Figure 3c,d; Figure S8, Supporting Information), which shows that the sulfur treatment also results in a reduction of the electron–hole recombination rate in the bulk of the semiconductor. This observation is supported by XPS depth profiling that shows that the sulfur is not only present at the surface of the semiconductor but penetrates deeper into the bulk of the film (Figure S9, Supporting Information). The initially high concentration of sulfur close to the surface decreases until it settles at $\approx$10 at.% ($\approx$40 nm deep into the sample).

Next, we used photoluminescence (PL) spectroscopy to understand the radiative recombination and to identify the passivation of nonradiative recombinative pathways of Sb_2Se_3 and sulfur-treated films. As the Sb_2Se_3 and sulfur-treated films exhibited low PL yield at room temperature, the PL spectra were acquired at 10 K (**Figure 4**a). The PL yield from Sb_2Se_3 was an order of magnitude lower than the sulfur-treated samples, indicating higher nonradiative losses in Sb_2Se_3 before sulfur treatment (inset Figure 4a). After sulfur treatment, these nonradiative recombination pathways are reduced, leading to a higher PL intensity. The PL spectra show a band-edge emission and a broad defect emission at lower energy. Investigation on the band-edge PL peak at 1.25 eV indicates that the transition is likely a free to bound state emission at 1.25 eV (as evidenced by no peak energy shift and the < 1 power law exponent of the PL intensity vs incident power plot (Figure S10, Supporting Information)).[20,21] The defect emission band extends over a broad energy range from 0.75 to 1.15 eV for Sb_2Se_3. The defect emission in the PL spectra at energies close to 0.8 eV was reduced due to sulfur treatment, suggesting a removal of
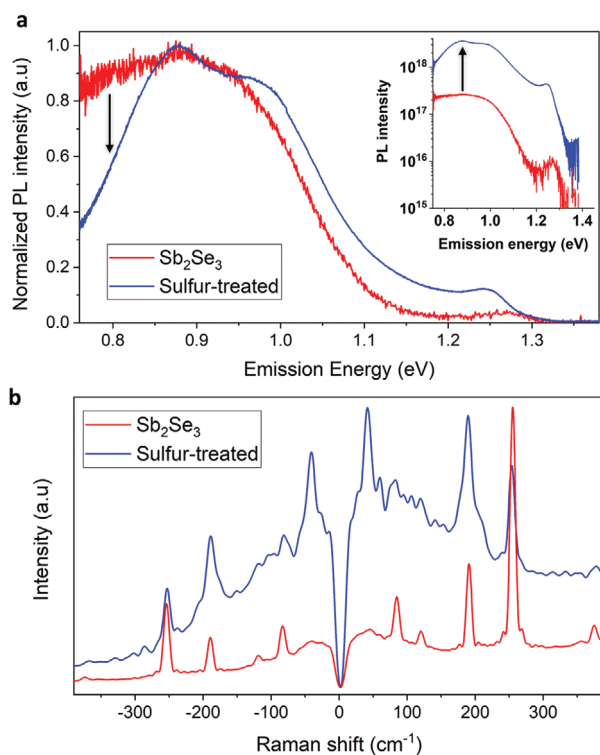
Figure 4. Defect passivation in sulfur-treated Sb_2Se_3 films. a) Low temperature (10 K) normalized PL spectra of Sb_2Se_3 and sulfur-treated films (excitation wavelength 633 nm). Inset shows the non-normalized PL intensity, illustrating the increased radiative recombination due to sulfur treatment. b) LFR spectra of Sb_2Se_3 films before and after defect passivation using sulfur.

a deep defect/trap state. The increased radiative recombination and decreased defect emission peak in sulfur-treated films coupled with a longer lifetime of the fast process and reduced bulk recombination rate observed from TRMC strongly suggest a passivation of deep defects in Sb_2Se_3. Recent computational studies have shown that Sb_{Se} antisite defects would occupy states at 0.4 eV above the valence band of Sb_2Se_3.[22] Due to the method of fabrication (selenization of an antimony metal film), we would expect such defects in our films. The relative suppression of defect emission at energies close to 0.8 eV when compared to the maximum PL emission suggests the passivation of Sb_{Se} antisite defects upon sulfur treatment of Sb_2Se_3 films.

Low-frequency Raman spectroscopy (LFR) can be used to probe the acoustic vibrational modes (AVM) of materials. Long-range order induces AVM enhancement thus revealing otherwise hidden LFR modes.[23,24] AVMs of Sb_2Se_3 have been extensively studied using DFT-based theoretical models. Figure 4b represents the LFR spectrum of the Sb_2Se_3 samples before and after sulfur treatment. Experimental LFR studies have optically resolved 15 of these theoretically predicted modes. The theoretical and experimental data agree within 5% deviation from theory.[25–27] The AVM modes reported in the literature (theoretically as well as experimentally) are compared with the modes we observed, in Table S3 (Supporting Information), and a graphical summary is presented in Figure S11 (Supporting Information). All of the LFR peaks observed prior

to sulfur treatment agree with the previously reported modes, the vibrational symmetries of which are well documented in the literature.[26,27] Upon sulfur treatment, two new AVM peaks emerge in the LFR at 95.18 and 141.41 cm^{-1}, corresponding to the simulated values of 94 and 142 cm^{-1}, respectively. We believe that this is the first time these modes have been resolved optically. We also observe that sulfur treatment enhances the AVMs at 106.53 and 118.83 cm^{-1}. Furthermore, the sulfur treatment induced a blue shift in the position of the LFR peaks from 60.03, 84.81, 191.20, and 256.03 cm^{-1}, observed prior to sulfur treatment, to lower wavenumbers of 59.05, 82.83, 189.74, and 253.07 cm^{-1}, respectively. Based on these observations, we propose that the sulfur treatment causes defect passivation in the Sb_2Se_3 crystal, resulting in reduced entropy of the crystal lattices and inducing long-range order in the system and enhancement of the hidden AVM modes of Sb_2Se_3.[28,29] Such enhancements and revelations of LFR peaks achieved upon inducing long-range order have been reported earlier.[30] It can therefore be inferred that the presence of sulfur at the defect site homogenizes the local phonon modes and energies, which results in long-range order, enhancement of hidden AVMs, and blue-shifts in the LFR peaks.

The defect passivation in sulfur-treated Sb_2Se_3 was further confirmed by investigating the photovoltage generated from Sb_2Se_3 PEC devices. To confirm the improvement of photovoltage upon sulfurization treatment of Sb_2Se_3, dual working electrode (DWE) devices were fabricated to directly probe the photovoltage generated by a p-n junction in a water-splitting photocathode (in our case Sb_2Se_3/TiO_2). As shown in Figure S12 (Supporting Information), the sulfurized sample (sulfur-treated/TiO_2/Pt) exhibits an improved onset potential of ≈ 350 mV versus V_{RHE}, compared to the non-treated Sb_2Se_3/TiO_2/Pt whose onset potential is ≈ 210 mV versus V_{RHE}. The J–ΔV (ΔV is the difference between the back contact potential WE1 and surface potential WE2) curves indicate that the V_{oc} generated by the Sb_2Se_3/TiO_2 heterojunction is ≈ 210 mV, which agrees well with the value of the onset potential for the standard J–V curve. Figure S12 (Supporting Information) clearly illustrates the improvement of photovoltage upon sulfurization treatment. Improvement in the photovoltage would indicate passivation of defects in the semiconductor and hence would be a key strategy for the improvement of the efficiency of Sb_2Se_3 for PEC and PV applications.[31]

3. Conclusions

A comprehensive investigation of the charge carrier dynamics of Sb_2Se_3 and the influence of sulfur treatment was performed using time-resolved microwave conductivity (TRMC), photoluminescence (PL) spectroscopy, and low-frequency Raman spectroscopy (LFR). The key finding is that upon sulfur treatment the carrier lifetime is increased (the electron-hole recombination rate is reduced) by the passivation of deep defects in Sb_2Se_3, which is evidenced by the longer time constant for the fast process in the TRMC upon sulfur treatment. On the other hand, the slow decay process sets in at earlier times for the sulfur treated samples pointing to a lower shallow trap density or narrower bandtail. Moreover, it was shown that the

sulfurization treatment reduces the electron–hole recombination rate across all excitation wavelengths (even for long wavelengths close to the bandgap energy and therefore penetrating deep into the bulk of the Sb_2Se_3) indicating that the treatment improves carrier lifetime in both the surface (Figure S13, Supporting Information) and bulk (Figure 3d). The passivation of deep defects in Sb_2Se_3 also increased radiative recombination, a key requisite for high-efficiency PV and PEC devices. The improved charge carrier dynamics is also supported by LFR that shows improved long-range order in the Sb_2Se_3 thin films upon sulfur treatment, as evidenced by the enhancement of hidden AVMs and blue-shifts in the LFR peaks. Understanding of defect passivation in Sb_2Se_3 provides crucial insights on the electronic properties of this emerging PV/PEC material, paving the way for highly efficient photoconversion devices.

Supporting Information

Supporting Information is available from the Wiley Online Library or from the author.

Acknowledgements

Conflict of Interest

The authors declare no conflict of interest.

Data Availability Statement

The data that support the findings of this study are available from the corresponding author upon reasonable request.

Keywords

[1] W. Yang, J. Moon, *J. Mater. Chem. A* **2019**, *7*, 20467.
[2] A. Mavlonov, T. Razykov, F. Raziq, J. Gan, J. Chantana, Y. Kawano, T. Nishimura, H. Wei, A. Zakutayev, T. Minemoto, X. Zu, S. Li, L. Qiao, *Sol. Energy* **2020**, *201*, 227.
[3] Y. Zhou, L. Wang, S. Chen, S. Qin, X. Liu, J. Chen, D.-J. Xue, M. Luo, Y. Cao, Y. Cheng, E. H. Sargent, J. Tang, *Nat Phot.* **2015**, *9*, 409.
[4] C. N. Savory, D. O. Scanlon, *J. Mater. Chem. A* **2019**, *7*, 10739.
[5] Y. Ma, B. Tang, W. Lian, C. Wu, X. Wang, H. Ju, C. Zhu, F. Fan, T. Chen, *J. Mater. Chem. A* **2020**, *8*, 6510.
[6] R. R. Prabhakar, W. Septina, S. Siol, T. Moehl, R. Wick-Joliat, S. D. Tilley, *J. Mater. Chem. A* **2017**, *5*, 23139.
[7] H. Zhou, M. Feng, M. Feng, X. Gong, D. Zhang, Y. Zhou, S. Chen, *Appl. Phys. Lett.* **2020**, *116*, 113902.
[8] C. Swiatkowski, A. Sanders, K. -D. Buhre, M. Kunst, *J. Appl. Phys.* **1995**, *78*, 1763.
[9] M. Kunst, F. Wünsch, D. Fuertes Marrón, A. Meeder, *Thin Solid Films* **2004**, *451–452*, 152.
[10] E. M. Hutter, G. E. Eperon, S. D. Stranks, T. J. Savenije, *J. Phys. Chem. Lett.* **2015**, *6*, 3082.
[11] A. Kay, M. Fiegenbaum-Raz, S. Müller, R. Eichberger, H. Dotan, R. van de Krol, F. F. Abdi, A. Rothschild, D. Friedrich, D. A. Grave, *Adv. Funct. Mater.* **2019**, *0*, 1901590.
[12] M. S. Prévot, X. A. Jeanbourquin, W. S. Bourée, F. Abdi, D. Friedrich, R. van de Krol, N. Guijarro, F. L.e Formal, K. Sivula, *Chem. Mater.* **2017**, *29*, 4952.
[13] F. F. Abdi, T. J. Savenije, M. M. May, B. Dam, R. van de Krol, *J. Phys. Chem. Lett.* **2013**, *4*, 2752.
[14] M. Kölbach, I. J. Pereira, K. Harbauer, P. Plate, K. Höflich, S. P. Berglund, D. Friedrich, R. van de Krol, F. F. Abdi, *Chem. Mater.* **2018**, *30*, 8322.
[15] A. Meeder, D. F. Marrón, M. C. Lux-Steiner, M. Kunst, *MRS Online Proc. Libr.* **2002**, *763*, 17.
[16] T. Tiedje, in *Hydrogenated Amorphous Silicon*, (Ed: J. I. Pankove), Vol. *763*, Elsevier, **1984**, p. 207.
[17] M. Kunst, S. Schwarz, *Recent Res. Devel. Sci. Tech. Semicond.* **2002**, *1*, 93.
[18] H. Feist, M. Kunst, *MRS Online Proc. Libr* **1997**, *467*, 227.
[19] D. Herm, H. Wetzel, M. Kunst, *MRS Online Proc. Libr.* **1990**, *192*, 651.
[20] T. Unold, L. Gütay, *Photoluminescence Analysis of Thin-Film Solar Cells* **2016**, pp. 275.
[21] C. Spindler, T. Galvani, L. Wirtz, G. Rey, S. Siebentritt, *J. Appl. Phys.* **2019**, *126*, 175703.
[22] A. Stoliaroff, A. Lecomte, O. Rubel, S. Jobic, X. Zhang, C. Latouche, X. Rocquefelte, *ACS Appl. Energy Mater.* **2020**, *3*, 2496.
[23] R. T. Sam, T. Umakoshi, P. Verma, *Appl. Phys. Express* **2020**, *13*, 072003.
[24] M. Inoue, H. Hisada, T. Koide, J. Carriere, R. Heyler, T. Fukami, *Org. Process Res. Dev.* **2017**, *21*, 262.
[25] A. Shongalova, M. R. Correia, B. Vermang, J. M. V. Cunha, P. M. P. Salomé, P. A. Fernandes, *MRS Commun.* **2018**, *8*, 865.
[26] N. Fleck, T. D. C. Hobson, C. N. Savory, J. Buckeridge, T. D. Veal, M. R. Correia, D. O. Scanlon, K. Durose, F. Jäckel, *J. Mater. Chem. A* **2020**, *8*, 8337.
[27] J. Ibáñez, J. A. Sans, C. Popescu, J. López-Vidrier, J. J. Elvira-Betanzos, V. P. Cuenca-Gotor, O. Gomis, F. J. Manjón, P. Rodríguez-Hernández, A. Muñoz, *J. Phys. Chem. C* **2016**, *120*, 10547.
[28] R. Gottesman, L. Gouda, B. S. Kalanoor, E. Haltzi, S. Tirosh, E. Rosh-Hodesh, Y. Tischler, A. Zaban, C. Quarti, E. Mosconi, F. De Angelis, *J. Phys. Chem. Lett.* **2015**, *6*, 2332.
[29] M. D. S. Lekgoathi, L. D. Kock, *Spectrochim. Acta Part A Mol. Biomol. Spectrosc.* **2016**, *153*, 651.
[30] V. H. Damle, L. Gouda, S. Tirosh, Y. R. Tischler, *ACS Appl. Energy Mater.* **2018**, *1*, 6707.
[31] S. Siebentritt, *Nat. Energy* **2017**, *2*, 840.